https://doi.org/10.20965/ijat.2010.p0346

Paper:

Kinematic Analysis and Design of 3-RPSR Parallel Mechanism with Triple Revolute Joints on the Base

Yukio Takeda*, Xiao Xiao*, Kazuya Hirose, Yoshiki Yoshida**, and Ken Ichiryu****

*Department of Mechanical Sciences and Engineering, Tokyo Institute of Technology
2-12-1 O-okayama, Meguro-ku, Tokyo 152-8552, Japan
E-mail: takeda@mech.titech.ac.jp
**Monozukuri Mechatro Research Laboratory, Kikuchi Seisakusho Co., Ltd.
2161-12 Miyama-cho, Hachioji-shi, Tokyo 192-0152, Japan
[Received February 14, 2010; accepted April 15, 2010]

The present paper proposes a new six-DOF parallel mechanism with three connecting chains. This mechanism can have a large angle of orientation of the output link. Joints in each connecting chain are arranged from the base in order of revolute, prismatic, spherical and revolute joints. All three revolute joints on the base are coaxial. With this structure, the output link can perform a full rotation around the vertical axis. The orientation capability of this mechanism is demonstrated. Equations for displacement analysis and the Jacobian matrix are derived. A design and prototype of this mechanism for a pipe-bender are shown.

Keywords: robotics, design engineering, kinematics, parallel mechanism, workspace, pipe bender

1. Introduction

Parallel mechanisms with six degrees of freedom (DOF) have attracted attention as appropriate mechanisms for performing tasks which require high accuracy, high acceleration, high rigidity, and high power. A huge number of researches have been done for such mechanisms with six connecting chains between the base and the output link, such as those with variable link lengths (Stewart platform type), fixed length links with linear drives, and fixed length links with rotary drives. They have been applied to motion simulators, machine tools, manipulators, etc. However, due to the limited orientation capability (small range of orientation angle of the output link) of these mechanisms, their applications are quite limited. Therefore, new designs of six-DOF parallel mechanisms that can achieve a large range of orientation angles of the output link are desperately needed.

The three components of angles representing the orientation of the output link are now classified into two groups. One is the angle around the axis perpendicular to the base plane (usually, the horizontal or vertical plane), and the other is that around the two axes on the base plane. In many applications, required ranges of angles in these two groups are 2π (former) and $\pm\pi/4$ (latter), respectively. The main reasons why six-DOF parallel mechanisms with six connecting chains can not achieve such a range of orientation angles are summarized as follows.

(1) Collisions among connecting chains are likely to occur during movement due to the large number of connecting chains.

(2) Since there is no common position/direction of joint axes in the mechanism, the common area of the orientation angles of the output link achieved by all the connecting chains becomes quite small and changes greatly according to the position of the output link.

(3) The range of motion of the spherical joint, which is frequently used at the end of the connecting chains with the output link for simplifying the structure, is small.

We propose a novel six-DOF parallel mechanism in order to solve these problems of orientation capability in six-DOF parallel mechanisms. Its main features are summarized as follows.

(a) There are three connecting chains.

(b) A revolute joint which is positioned at the center of the base and directed in perpendicular to the base plane is commonly used in each connecting chain. With this composition, the orientation angle of the output link around the axis of these joints becomes independent of the other two angles.

(c) Revolute joints, which usually have a large range of motion, are used at the end of the connecting chains with the output link in order that the output link be able to have a large range of orientation angle, while spherical joints are used at other places to simplify the composition of the mechanism.

As an example of a mechanism that has these features, we propose the 3-RPSR mechanism with triple revolute joints on the base shown in **Fig. 1**, in which only one connecting chain is clearly shown. In its connecting chain, links are connected by a revolute (R), prismatic (P), spherical (S) and revolute joints from the base to the output link. The three revolute joints on the base are coaxial.

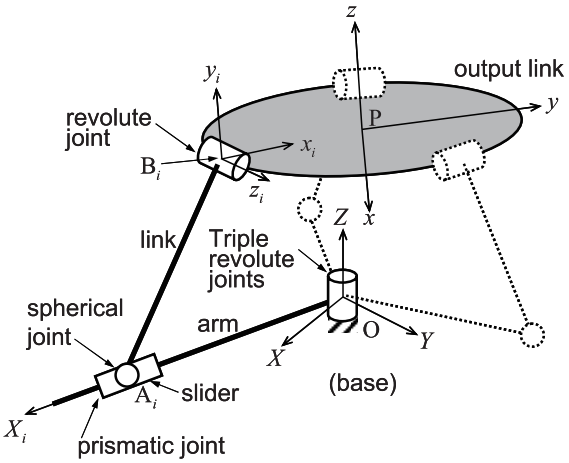

Fig. 1. 3-RPSR mechanism with triple revolute joints.

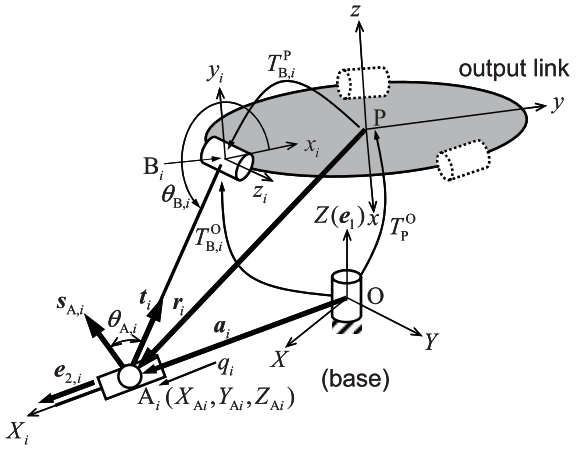

Fig. 2. Definition of symbols.

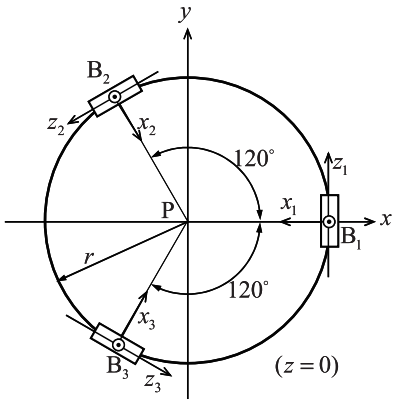

Fig. 3. Location of revolute joints on the output link.

A six-DOF parallel mechanism composed of six connecting chains with six coaxial vertical revolute joints on the base has been invented [1], and put into practical use [2]. However, its range of orientation angle of the output link around the horizontal axes is limited to $\pm\pi/12$, which is on the same level as that of other six-DOF parallel mechanisms. As for mechanisms composed of three connecting chains, no reports regarding mechanisms with a large range of orientation angle have been found by the authors. On the other hand, position-orientation decoupled mechanisms [3], and hybrid mechanisms composed of a translational parallel mechanism [4] and a pure rotational parallel mechanism [5] each with three-DOF are considered to be good candidates for good orientation capability. However, no reports regarding mechanisms with orientation capabilities such as full rotation around the vertical axis have been found.

In the present paper, kinematic analysis of a novel six-DOF parallel mechanism with triple revolute joints on the base, 3-RPSR mechanism, is presented, and a case study on the design of a pipe bender using this mechanism is discussed.

2. 3-RPSR Mechanism

2.1. Description of the Mechanism

The kinematic structure of the 3-RPSR mechanism is shown in **Fig. 1**. As mentioned above, this mechanism is composed of the base, output link, and three connecting chains. In each connecting chain, the base, arm, slider, link, and output link are connected by revolute, prismatic, spherical and revolute joints. The axes of all revolute joints which connect the connecting chains with the base are identical to the Z axis of the base coordinate system O-XYZ. The three connecting chains have the same structure and dimensions, and they are symmetrically located with respect to O-XYZ and the moving coordinate system fixed on the output link P-xyz. P represents the reference point on the output link. The revolute joints on the base and the prismatic joints are active joints.

As shown in **Figs. 2**-**5**, two moving coordinate systems O-$X_iY_iZ_i$ and B_i-$x_iy_iz_i$ are considered, while i represents the connecting chain number ($i = 1,2,3$). O-$X_iY_iZ_i$ is fixed on the arm, and the X_i axis is identical to the axis of the prismatic joint. B_i-$x_iy_iz_i$ is fixed at B_i on the output link, and the z_i axis is identical to the axis of the revolute joint on the output link. The center of the spherical joints are denoted as A_i.

Kinematic constants are r (radius of the location circle of revolute joints on the output link), l (link length $\overline{A_iB_i}$), and β_B (the angle between the axis of the prismatic joint (X_i) and the base plane (XY plane)).

Angular displacement of the revolute joint on the base, displacement of the prismatic joint, and angular displacement of the revolute joint on the output link in the i-th connecting chain are denoted as θ_i, q_i and $\theta_{B,i}$, respectively. A unit vector which represents the direction of the swing center of the spherical joint is denoted as $\boldsymbol{s}_{A,i}$. The angle between $\overrightarrow{A_iB_i}$ and $\boldsymbol{s}_{A,i}$, which represents the swing angle of the spherical joint, is denoted as $\theta_{A,i}$. Position vectors $\boldsymbol{a}_i$ and $\boldsymbol{r}_i$, unit vectors $\boldsymbol{t}_i$ (direction of the link A_i B_i), $\boldsymbol{e}_1$ (direction of the revolute joint axis on the base), $\boldsymbol{e}_{2,i}$ (direction of the prismatic joint axis), and $\boldsymbol{z}_i$ (direction of the revolute joint axis at B_i) are defined as shown in **Figs. 2** and **4**.

Relationships among four coordinate systems O-XYZ, P-xyz, B_i-$x_iy_iz_i$ and O-$X_iY_iZ_i$ are described using 4×4

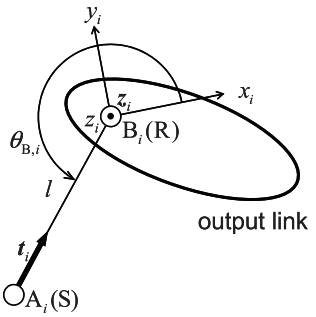

Fig. 4. Definition of symbols related to the revolute joints on the output link.

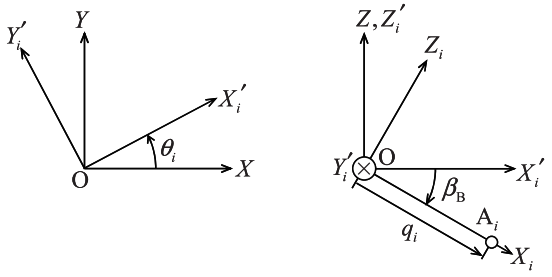

Fig. 5. Definition of joint displacements θ_i and q_i.

transformation matrices $T^{\mathrm{P}}_{\mathrm{B},i}$, $T^{\mathrm{O}}_{\mathrm{B},i}$, $T^{\mathrm{O}}_{\mathrm{P}}$ and $T^{\mathrm{O}}_{\mathrm{O},i}$ as follows.

$$\begin{bmatrix} 1 \\ \boldsymbol{x}^{\mathrm{P}} \end{bmatrix} = T^{\mathrm{P}}_{\mathrm{B},i} \begin{bmatrix} 1 \\ \boldsymbol{x}^{\mathrm{B},i} \end{bmatrix},$$

$$\begin{bmatrix} 1 \\ \boldsymbol{x}^{\mathrm{O}} \end{bmatrix} = T^{\mathrm{O}}_{\mathrm{P}} \begin{bmatrix} 1 \\ \boldsymbol{x}^{\mathrm{P}} \end{bmatrix} = T^{\mathrm{O}}_{\mathrm{P}} T^{\mathrm{P}}_{\mathrm{B},i} \begin{bmatrix} 1 \\ \boldsymbol{x}^{\mathrm{B},i} \end{bmatrix} = T^{\mathrm{O}}_{\mathrm{B},i} \begin{bmatrix} 1 \\ \boldsymbol{x}^{\mathrm{B},i} \end{bmatrix},$$

$$\begin{bmatrix} 1 \\ \boldsymbol{x}^{\mathrm{O}} \end{bmatrix} = T^{\mathrm{O}}_{\mathrm{O},i} \begin{bmatrix} 1 \\ \boldsymbol{x}^{\mathrm{O},i} \end{bmatrix} \quad \ldots\ldots\ldots\ldots \quad (1)$$

$$T^{\mathrm{P}}_{\mathrm{B},i} = \begin{bmatrix} 1 & 0\,0\,0 \\ \boldsymbol{b}^{\mathrm{P}}_i & R^{\mathrm{P}}_{\mathrm{B},i} \end{bmatrix}, \; T^{\mathrm{O}}_{\mathrm{P}} = \begin{bmatrix} 1 & 0\,0\,0 \\ \boldsymbol{P}^{\mathrm{O}} & R^{\mathrm{O}}_{\mathrm{P}} \end{bmatrix},$$

$$T^{\mathrm{O}}_{\mathrm{B},i} = \begin{bmatrix} 1 & 0\,0\,0 \\ \boldsymbol{B}^{\mathrm{O}}_i & R^{\mathrm{O}}_{\mathrm{B},i} \end{bmatrix}, \; T^{\mathrm{O}}_{\mathrm{O},i} = \begin{bmatrix} 1 & 0\,0\,0 \\ \boldsymbol{0} & R^{\mathrm{O}}_{\mathrm{O},i} \end{bmatrix}$$

Here, $\boldsymbol{x}^{\mathrm{O}}$, $\boldsymbol{x}^{\mathrm{P}}$, $\boldsymbol{x}^{\mathrm{B},i}$, and $\boldsymbol{x}^{\mathrm{O},i}$ represent the descriptions of vector $\boldsymbol{x}$ written in O-XYZ, P-xyz, B$_i$-$x_iy_iz_i$, and O-$X_iY_iZ_i$ coordinate systems, respectively. $T^{\mathrm{P}}_{\mathrm{B},i}$ is determined by the kinematic constants.

The orientation of the output link is represented by the three angles θ_y, θ_z, and ψ, shown in **Fig. 6**. By rotating the base coordinate system O-XYZ by θ_y around $\boldsymbol{e}_{\mathrm{R1}}$, the Z axis directs to $\boldsymbol{e}_{\mathrm{R2}}$. The projected vector of $\boldsymbol{e}_{\mathrm{R2}}$ on the XY plane is in the direction of θ_z measured from the X axis. ψ is the angle around $\boldsymbol{e}_{\mathrm{R2}}$. The rotation matrix R is described using these three angles as

$$R = R_1 R_2 R_1^{\mathrm{T}} R_3. \quad \ldots\ldots\ldots\ldots \quad (2)$$

Here,

$$R_1 = \begin{bmatrix} \sin\theta_z & \cos\theta_z & 0 \\ -\cos\theta_z & \sin\theta_z & 0 \\ 0 & 0 & 1 \end{bmatrix},$$

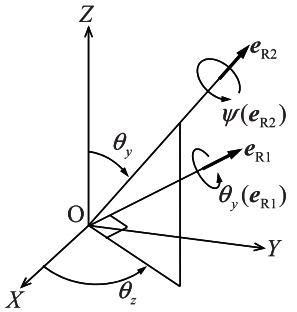

Fig. 6. Definition of orientation angles θ_y, θ_z, and ψ.

$$R_2 = \begin{bmatrix} 1 & 0 & 0 \\ 0 & \cos\theta_y & \sin\theta_y \\ 0 & -\sin\theta_y & \cos\theta_y \end{bmatrix},$$

$$R_3 = \begin{bmatrix} \cos\psi & -\sin\psi & 0 \\ \sin\psi & \cos\psi & 0 \\ 0 & 0 & 1 \end{bmatrix}.$$

2.2. Features of the Mechanism

The 3-RPSR mechanism proposed in this paper can achieve a large angle of inclination of the output link (large θ_y) while being able to perform full rotation of the output link around the Z axis. To show this orientation capability, some characteristic configurations of this mechanism are shown in projective planes in **Fig. 7**. **Fig. 7 (a)** shows the configuration at the home pose ($X = Y = 0, Z = Z_{\mathrm{O}}, \theta_y = \theta_z = \psi = 0$). As shown by arrows in **Fig. 7 (b)**, **(c)**, and **(e)**, by combining input motions of the revolute joints and prismatic joints, the output link can achieve a large angle of inclination in any direction. As described in the introduction, the maximum swing angle of the spherical joint is limited (up to $\pm 2\pi/9$ rad). From offset poses such that in **Fig. 7 (d)** (at this pose, $X_P/r = 0.5$), this mechanism can achieve a large inclination of the output link, as shown in **Fig. 7 (e)**, not only by the combination of rotation and translation of inputs, but by using an appropriately designed angle of the slider β_{B} even though the swing angle of spherical joints is limited.

When the mechanism performs rotation of the output link around the Z axis, a large amount of power can be output because the three actuators at the base operate in parallel.

3. Inverse Displacement Analysis

3.1. Basic Equations

Since the center of spherical joint A$_i$ moves on the circular cone defined by the vertex O, the Z axis and angle β_{B}, the coordinate of A$_i(X_{A,i}, Y_{A,i}, Z_{A,i})$, which is written in O-$XYZ$, satisfies the following equation.

$$(X^2_{\mathrm{A},i} + Y^2_{\mathrm{A},i}) \tan^2\beta_{\mathrm{B}} = Z^2_{\mathrm{A},i} \quad \ldots\ldots\ldots \quad (3)$$

On the other hand, since A$_i$ lies on the circle of center B$_i$ and radius l, the coordinate of A$_i(x_i, y_i, z_i)$ written in B$_i$

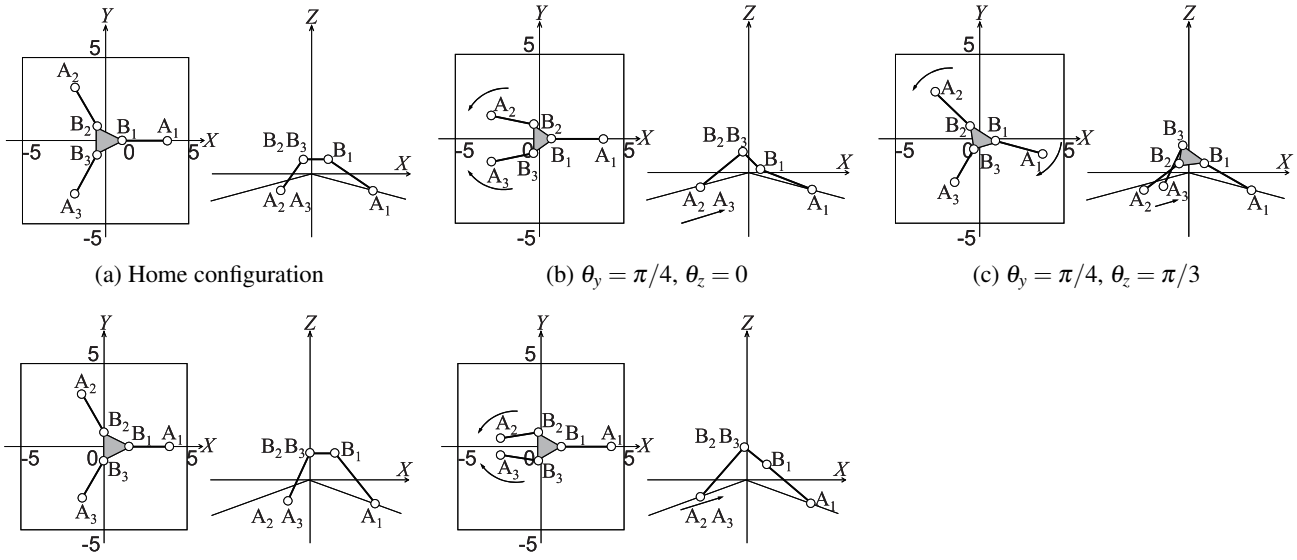

(a) Home configuration (b) $\theta_y = \pi/4$, $\theta_z = 0$ (c) $\theta_y = \pi/4$, $\theta_z = \pi/3$

(d) $X = 0.5$, $Z = Z_O + 0.5$ (e) $X = 0.5$, $Z = Z_O + 0.5$, $\theta_y = \pi/4$, $\theta_z = 0$

Fig. 7. Characteristic configurations to demonstrate the orientation capability of the 3-RPSR mechanism ($r = 1$).

-$x_i y_i z_i$ satisfies

$$x_i^2 + y_i^2 = l^2,\ z_i = 0. \quad \ldots\ldots\ldots\ldots \quad (4)$$

When the matrix $T^{\mathrm{O}}_{\mathrm{B},i}$ is written as

$$T^{\mathrm{O}}_{\mathrm{B},i} = \begin{bmatrix} 1 & 0 & 0 & 0 \\ X_{\mathrm{B},i} & a_{11} & a_{12} & a_{13} \\ Y_{\mathrm{B},i} & a_{21} & a_{22} & a_{23} \\ Z_{\mathrm{B},i} & a_{31} & a_{32} & a_{33} \end{bmatrix} \quad \ldots\ldots \quad (5)$$

Eq. (3) is rewritten in the following form.

$$\begin{aligned} &\left\{(X_{\mathrm{B},i} + a_{11}x_i + a_{12}y_i + a_{13}z_i)^2\right. \\ &\left.+(Y_{\mathrm{B},i} + a_{21}x_i + a_{22}y_i + a_{23}z_i)^2\right\}\tan^2\beta_{\mathrm{B}} \\ &= (Z_{\mathrm{B},i} + a_{31}x_i + a_{32}y_i + a_{33}z_i)^2 \quad \ldots\ldots \quad (6) \end{aligned}$$

From Eqs. (4) and (6), the following simultaneous equation with respect to (x_i, y_i, z_i) is obtained.

$$\left.\begin{aligned} &x_i^2 + y_i^2 = l^2 \\ &\left\{(X_{\mathrm{B},i} + a_{11}x_i + a_{12}y_i)^2\right. \\ &\left.+(Y_{\mathrm{B},i} + a_{21}x_i + a_{22}y_i)^2\right\}\tan^2\beta_{\mathrm{B}} \\ &= (Z_{\mathrm{B},i} + a_{31}x_i + a_{32}y_i)^2 \end{aligned}\right\} \quad \ldots\ldots \quad (7)$$

Since the coordinate of B_i ($X_{\mathrm{B},i}$, $Y_{\mathrm{B},i}$, $Z_{\mathrm{B},i}$) in O-XYZ is easily calculated from the position of P (X_{P}, Y_{P}, Z_{P}) and the orientation of the output link (θ_y, θ_z, ψ) in the inverse displacement analysis, we consider these as known parameters here. Eq. (7) results in a quartic equation. In our study, we solve Eq. (7) numerically as follows, taking into consideration discrimination of solutions.

The solution of y_i in the second equation in Eq. (7) for assumed x_i is obtained as

$$y_i = \frac{-(B + Cx_i) \pm \sqrt{(B + Cx_i)^2 - A(Dx_i^2 + 2Ex_i + F)}}{A} \quad \ldots\ldots\ldots\ldots \quad (8)$$

where

$$\left.\begin{aligned} A &= a_{12}^2\tan^2\beta_{\mathrm{B}} + a_{22}^2\tan^2\beta_{\mathrm{B}} - a_{32}^2 \\ B &= a_{12}X_{\mathrm{B},i}\tan^2\beta_{\mathrm{B}} + a_{22}Y_{\mathrm{B},i}\tan^2\beta_{\mathrm{B}} - a_{32}Z_{\mathrm{B},i} \\ C &= a_{11}a_{12}\tan^2\beta_{\mathrm{B}} + a_{21}a_{22}\tan^2\beta_{\mathrm{B}} - a_{31}a_{32} \\ D &= a_{11}^2\tan^2\beta_{\mathrm{B}} + a_{21}^2\tan^2\beta_{\mathrm{B}} - a_{31}^2 \\ E &= a_{11}X_{\mathrm{B},i}\tan^2\beta_{\mathrm{B}} + a_{21}Y_{\mathrm{B},i}\tan^2\beta_{\mathrm{B}} - a_{31}Z_{\mathrm{B},i} \\ F &= X_{\mathrm{B},i}^2\tan^2\beta_{\mathrm{B}} + Y_{\mathrm{B},i}^2\tan^2\beta_{\mathrm{B}} - Z_{\mathrm{B},i}^2 \end{aligned}\right\}. \quad (9)$$

From the first equation in Eq. (7), the following function

$$f(x_i) = x_i^2 + y_i^2 - l^2 \quad \ldots\ldots\ldots\ldots \quad (10)$$

is considered. By using this function, the solution of Eq. (7) is iteratively searched until the following equation is satisfied.

$$f(x_i) = 0 \quad \ldots\ldots\ldots\ldots \quad (11)$$

Description of the coordinate of A_i in O-XYZ is obtained from the solution of (x_i, y_i, z_i) using $T^{\mathrm{O}}_{\mathrm{B},i}$ in Eq. (1). Using this coordinate $(X_{A,i}, Y_{A,i}, Z_{A,i})$, the joint displacements are obtained. The calculation procedure will be explained in 3.3.

3.2. Discrimination of Solutions

Though in theory there exist four solutions in Eq. (7), only one solution among them is effective. Discrimination of the solutions is done through the following two steps.

(1) From the geometrical condition, only the two solutions which satisfy $Z_{\mathrm{A},i} \leq 0$ are selected.

(2) Two solutions $\mathrm{A}_{i,1}$ and $\mathrm{A}_{i,2}$ in $x_i y_i$ plane ($z_i = 0$) are shown in **Fig. 8** as the intersection of S_i (the second equation of Eq. (7)) and a circle of radius l (the first equation of Eq. (7)). We consider a point T_i, at which the distance from B_i is minimum on S_i. When Eq. (7)

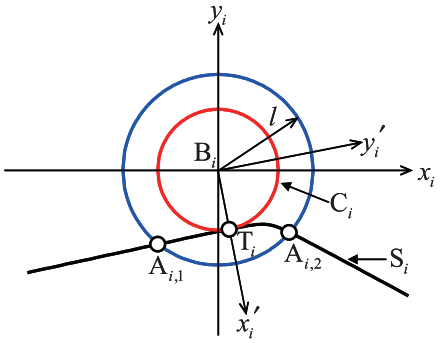

Fig. 8. Discrimination of solutions.

has a multiple solution, the mechanism is located at a singular point, and $A_{i,1}$ and $A_{i,2}$ coincide with T_i. Once the mechanism is assembled, the solution of the inverse displacement analysis can not jump from $A_{i,1}$ to $A_{i,2}$ through T_i and vice versa. Now, a coordinate system B_i-$x_i'y_i'$, which is obtained by setting the direction of $\overrightarrow{B_iT_i}$ as x_i' axis, is considered. The solutions can be discriminated by the y_i' coordinate (positive or negative) of the solutions. In our study, the negative y_i' solution is chosen.

3.3. Calculation of Joint Displacement

From the coordinate of $A_i(X_{A,i}, Y_{A,i}, Z_{A,i})$ in O-XYZ, the displacement of active joints θ_i and q_i is calculated as follows:

$$\cos\theta_i = \frac{X_{A,i}}{\sqrt{X_{A,i}^2+Y_{A,i}^2}},\ \sin\theta_i = \frac{Y_{A,i}}{\sqrt{X_{A,i}^2+Y_{A,i}^2}} \quad . \quad (12)$$

$$q_i = \sqrt{X_{A,i}^2+Y_{A,i}^2+Z_{A,i}^2}. \quad . \quad (13)$$

$\boldsymbol{t}_i^{O}$, unit vector in the direction of $\overrightarrow{A_iB_i}$ represented in O-XYZ, is easily obtained from $(X_{B,i}, Y_{B,i}, Z_{B,i})$ and $(X_{A,i}, Y_{A,i}, Z_{A,i})$, which have already been calculated. $\boldsymbol{t}_i^{B,i}$, unit vector in the direction of $\overrightarrow{A_iB_i}$ represented in B_i-$x_iy_iz_i$, is obtained by the following equation using the rotation matrix $R_{B,i}^{O}$.

$$\boldsymbol{t}_i^{B,i} = \left(R_{B,i}^{O}\right)^{T}\boldsymbol{t}_i^{O} \quad . \quad (14)$$

The angular displacement $\theta_{B,i}$ is calculated by

$$\cos\theta_{B,i} = -t_{i,x}^{B,i},\ \sin\theta_{B,i} = -t_{i,y}^{B,i} \quad . \quad (15)$$

where $\boldsymbol{t}_i^{B,i} = \left[t_{i,x}^{B,i}\ t_{i,y}^{B,i}\ t_{i,z}^{B,i}\right]^{T}$.

A unit vector $\boldsymbol{t}_i^{O,i}$, which is the description of $\boldsymbol{t}_i$ in O-$X_iY_iZ_i$, is obtained by

$$\boldsymbol{t}_i^{O,i} = \left(R_{O,i}^{O}\right)^{T}\boldsymbol{t}_i^{O} \quad . \quad (16)$$

where

$$R_{O,i}^{O} = \begin{bmatrix} \cos\theta_i & -\sin\theta_i & 0 \\ \sin\theta_i & \cos\theta_i & 0 \\ 0 & 0 & 1 \end{bmatrix}\begin{bmatrix} \cos\beta_B & 0 & \sin\beta_B \\ 0 & 1 & 0 \\ -\sin\beta_B & 0 & \cos\beta_B \end{bmatrix}$$

$$= \begin{bmatrix} \cos\theta_i\cos\beta_B & -\sin\theta_i & \cos\theta_i\sin\beta_B \\ \sin\theta_i\cos\beta_B & \cos\theta_i & \sin\theta_i\sin\beta_B \\ -\sin\beta_B & 0 & \cos\beta_B \end{bmatrix}. \quad . \quad (17)$$

The swing angle of spherical joint $\theta_{A,i}$ is calculated using $\boldsymbol{t}_i^{O,i}$ and $\boldsymbol{s}_{A,i}^{O,i}$ as

$$\theta_{A,i} = \cos^{-1}\left\{\boldsymbol{s}_{A,i}^{O,i},\ \boldsymbol{t}_i^{O,i}\right\}, \quad . \quad (18)$$

where $\{\ ,\ \}$ represents the inner product of vectors. $\boldsymbol{s}_{A,i}^{O,i}$ is the constant vector given or determined at design.

When $\beta_B = 0$, the equation for the inverse displacement analysis results in a quadratic equation in one variable for each connecting chain.

4. Jacobian Matrix

External force and moment exerted on the output link are denoted as $\boldsymbol{F}^{O} = [F_X\ F_Y\ F_Z]^{T}$ and $\boldsymbol{M}^{O} = [M_X\ M_Y\ M_Z]^{T}$, respectively. The force and moment acting from each connecting chain to the output link are divided into two force components acting at A_i. They are a force in the direction of $\overrightarrow{A_iB_i}$ and that along the axis of the revolute joint at B_i. The magnitudes of these force components are denoted as $f_{1,i}$ and $f_{2,i}$, respectively. The equilibrium equation on force and moment with respect to the output link is written as

$$\begin{bmatrix} \boldsymbol{F}^{O} \\ \boldsymbol{M}^{O} \end{bmatrix} = -J_1\boldsymbol{f}, \quad . \quad (19)$$

where

$$J_1 = \begin{bmatrix} \boldsymbol{t}_1^{O} & \boldsymbol{t}_2^{O} & \boldsymbol{t}_3^{O} & \boldsymbol{z}_1^{O} & \boldsymbol{z}_2^{O} & \boldsymbol{z}_3^{O} \\ \boldsymbol{r}_1^{O}\times\boldsymbol{t}_1^{O} & \boldsymbol{r}_2^{O}\times\boldsymbol{t}_2^{O} & \boldsymbol{r}_3^{O}\times\boldsymbol{t}_3^{O} & \boldsymbol{r}_1^{O}\times\boldsymbol{z}_1^{O} & \boldsymbol{r}_2^{O}\times\boldsymbol{z}_2^{O} & \boldsymbol{r}_3^{O}\times\boldsymbol{z}_3^{O} \end{bmatrix}$$

$$\boldsymbol{f} = \left[f_{1,1}\ f_{1,2}\ f_{1,3}\ f_{2,1}\ f_{2,2}\ f_{2,3}\right]^{T}.$$

$\boldsymbol{r}_i^{O}$ and $\boldsymbol{z}_i^{O}$ are the position vector of A_i from P and the unit vector representing the axis of revolute joint at B_i, respectively. Unit vectors representing directions of axes of active joints $\boldsymbol{e}_1^{O}$(revolute) and $\boldsymbol{e}_{2,i}^{O}$(prismatic) are written as

$$\boldsymbol{e}_1^{O} = \begin{bmatrix} 0 \\ 0 \\ 1 \end{bmatrix},\ \boldsymbol{e}_{2,i}^{O} = \begin{bmatrix} \cos\beta_B\cos\theta_i \\ \cos\beta_B\sin\theta_i \\ -\sin\beta_B \end{bmatrix}. \quad . \quad (20)$$

Driving torque $\tau_{1,i}$ around the axis $\boldsymbol{e}_1^{O}$ which corresponds to the force acting from i-th connecting chain to the output link at A_i is obtained by

$$\tau_{1,i} = \left\{\boldsymbol{a}_i^{O}\times(f_{1,i}\boldsymbol{t}_i^{O}+f_{2,i}\boldsymbol{z}_i^{O}),\ \boldsymbol{e}_1^{O}\right\}$$
$$= \left\{\boldsymbol{a}_i^{O}\times\boldsymbol{t}_i^{O},\ \boldsymbol{e}_1^{O}\right\}f_{1,i} + \left\{\boldsymbol{a}_i^{O}\times\boldsymbol{z}_i^{O},\ \boldsymbol{e}_1^{O}\right\}f_{2,i}. \quad (21)$$

Driving force $\tau_{2,i}$ along the axis $\boldsymbol{e}_{2,i}^{O}$ is obtained by

$$\tau_{2,i} = \left\{f_{1,i}\boldsymbol{t}_i^{O}+f_{2,i}\boldsymbol{z}_i^{O},\ \boldsymbol{e}_{2,i}^{O}\right\}$$
$$= \left\{\boldsymbol{t}_i^{O},\boldsymbol{e}_{2,i}^{O}\right\}f_{1,i} + \left\{\boldsymbol{z}_i^{O},\boldsymbol{e}_{2,i}^{O}\right\}f_{2,i}. \quad . \quad (22)$$

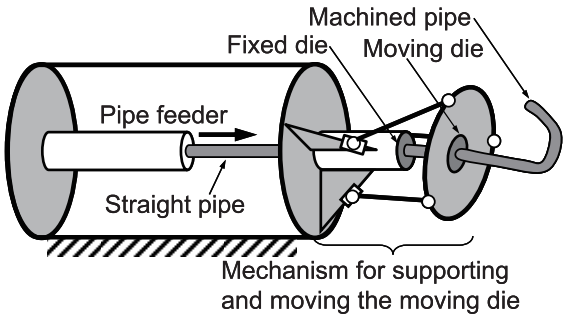

Fig. 9. Composition of a pipe bender.

The relations in Eqs. (21) and (22) are summarized as

$$\boldsymbol{\tau} = J_2 \boldsymbol{f} \quad \ldots\ldots\ldots\ldots\ldots\ldots (23)$$

where

$$J_2 = \begin{bmatrix} \{\boldsymbol{a}_1^{\mathrm{O}} \times \boldsymbol{t}_1^{\mathrm{O}}, \boldsymbol{e}_1^{\mathrm{O}}\} & 0 & 0 & \{\boldsymbol{a}_1^{\mathrm{O}} \times \boldsymbol{z}_1^{\mathrm{O}}, \boldsymbol{e}_1^{\mathrm{O}}\} & 0 & 0 \\ 0 & \{\boldsymbol{a}_2^{\mathrm{O}} \times \boldsymbol{t}_2^{\mathrm{O}}, \boldsymbol{e}_1^{\mathrm{O}}\} & 0 & 0 & \{\boldsymbol{a}_2^{\mathrm{O}} \times \boldsymbol{z}_2^{\mathrm{O}}, \boldsymbol{e}_1^{\mathrm{O}}\} & 0 \\ 0 & 0 & \{\boldsymbol{a}_3^{\mathrm{O}} \times \boldsymbol{t}_3^{\mathrm{O}}, \boldsymbol{e}_1^{\mathrm{O}}\} & 0 & 0 & \{\boldsymbol{a}_3^{\mathrm{O}} \times \boldsymbol{z}_3^{\mathrm{O}}, \boldsymbol{e}_1^{\mathrm{O}}\} \\ \{\boldsymbol{t}_1^{\mathrm{O}}, \boldsymbol{e}_{2,1}^{\mathrm{O}}\} & 0 & 0 & \{\boldsymbol{z}_1^{\mathrm{O}}, \boldsymbol{e}_{2,1}^{\mathrm{O}}\} & 0 & 0 \\ 0 & \{\boldsymbol{t}_2^{\mathrm{O}}, \boldsymbol{e}_{2,2}^{\mathrm{O}}\} & 0 & 0 & \{\boldsymbol{z}_2^{\mathrm{O}}, \boldsymbol{e}_{2,2}^{\mathrm{O}}\} & 0 \\ 0 & 0 & \{\boldsymbol{t}_3^{\mathrm{O}}, \boldsymbol{e}_{2,3}^{\mathrm{O}}\} & 0 & 0 & \{\boldsymbol{z}_3^{\mathrm{O}}, \boldsymbol{e}_{2,3}^{\mathrm{O}}\} \end{bmatrix}$$

$$\boldsymbol{\tau} = \begin{bmatrix} \tau_{1,1} & \tau_{1,2} & \tau_{1,3} & \tau_{2,1} & \tau_{2,2} & \tau_{2,3} \end{bmatrix}^{\mathrm{T}}.$$

From Eqs. (19) and (23), the following equation is obtained.

$$\begin{bmatrix} \boldsymbol{F}^{\mathrm{O}} \\ \boldsymbol{M}^{\mathrm{O}} \end{bmatrix} = -J\tau,\ J = J_1 J_2^{-1} \quad \ldots\ldots\ldots (24)$$

The matrix J in Eq. (24) is the Jacobian matrix. Using J, inverse velocity analysis can be done by

$$\dot{\boldsymbol{q}} = J^{\mathrm{T}} \dot{\boldsymbol{X}}^{\mathrm{O}} \quad \ldots\ldots\ldots\ldots\ldots\ldots (25)$$

where $\dot{\boldsymbol{q}} = \begin{bmatrix} \dot{\theta}_1 & \dot{\theta}_2 & \dot{\theta}_3 & \dot{q}_1 & \dot{q}_2 & \dot{q}_3 \end{bmatrix}^{\mathrm{T}}$
and $\dot{\boldsymbol{X}}^{\mathrm{O}} = \begin{bmatrix} \dot{X}_{\mathrm{P}} & \dot{Y}_{\mathrm{P}} & \dot{Z}_{\mathrm{P}} & \dot{\Theta}_X & \dot{\Theta}_Y & \dot{\Theta}_Z \end{bmatrix}^{\mathrm{T}}$
are input velocity and output velocity, respectively.

5. Kinematic Design for a Pipe Bender

5.1. Problem Statement

The authors are developing a novel pipe bender using parallel mechanism with six DOF, as shown in **Fig. 9** [6]. Parallel mechanism is used to move the moving die relative to the fixed die. This motion is controlled to synchronize with that of the pipe feeder. A Stewart platform-type parallel mechanism has been applied to this pipe bender, and pipe with three-dimensional shape has been manufactured at Kikuchi Seisakusho Co., Ltd [7]. However, a mechanism which can achieve a wide orientation angle has been strongly needed for the manufacture of more complicated objects. Therefore, taking into consideration its orientation capability, we designed a 3-RPSR mechanism for a pipe bender.

Table 1. Specifications and result of mechanism design.

S_X / r	0.5	$\boldsymbol{s}_{\mathrm{A},i}^{\mathrm{O},i}$	$[-0.941\ 0\ 0.339]^{\mathrm{T}}$
S_Z / r	0.5	$w_{\max}$	6.18
$\theta_{y,\max}$	$\pi/4$ rad	$w_{\min}$	0.61
l / r	3.3	$\theta_{\mathrm{A},\max}$	0.35 rad
β_{B}	$\pi/12$ rad	$q_{\max}$	4.21
Z_{O} / r	0.891	$q_{\min}$	2.22

(1) Prescribed workspace

Taking into consideration the movement typically required of a moving die in bending pipe, the prescribed workspace was derived from the following set of paths.

$$\left.\begin{array}{l} \theta_z : [0,\ 2\pi],\ X'' : [0,\ S_X] \\ X = X'' \cos\theta_z \\ Y = X'' \sin\theta_z \\ Z = Z_{\mathrm{O}} - S_Z + 2\dfrac{S_Z}{S_X} X'' \\ \theta_y = \dfrac{\theta_{y,\max}}{S_X} X'' \\ \psi = 0 \end{array}\right\} \quad \ldots\ldots\ldots (26)$$

Here, X'' is obtained by rotating the X axis by θ_z around the Z axis. S_X, S_Z, and $\theta_{y,\max}$ are given as design specifications.

(2) Evaluation indices and conditions

The following three indices were defined.

(i) Maximum and minimum values of determinant of Jacobian matrix J in Eq. (24), $w_{\max}$ and $w_{\min}$.

(ii) Maximum swing angle of spherical joint, $\theta_{\mathrm{A},\max}$.

(iii) Maximum and minimum displacement of prismatic joint, $q_{\max}$ and $q_{\min}$.

In order to obtain useful mechanisms, the following conditions were taken into consideration (r = 1).

$$w_{\max} \le 10,\ w_{\min} \ge 0.1,\ \theta_{\mathrm{A},\max} \le 2\pi/9\,\mathrm{rad}$$

$$q_{\max} \le 5,\ q_{\min} \ge 1$$

(3) Design conditions

Values of parameters to define the size of the prescribed workspace were given as shown in **Table 1**. $\boldsymbol{s}_{\mathrm{A},i}^{\mathrm{O},i}$, which represents the center of swing of spherical joint, was defined so that $\theta_{\mathrm{A},i}$ equals zero when the output link is in its home pose ($X_{\mathrm{P}} = Y_{\mathrm{P}} = 0$, $Z_{\mathrm{P}} = Z_{\mathrm{O}}$, $\theta_y = \theta_z = \psi = 0$). Ranges of parameters were given as $l : [1, 6]r$, $Z_{\mathrm{O}} : [0.2l, 0.6l]$, $\beta_{\mathrm{B}} : [0, \pi/6]$.

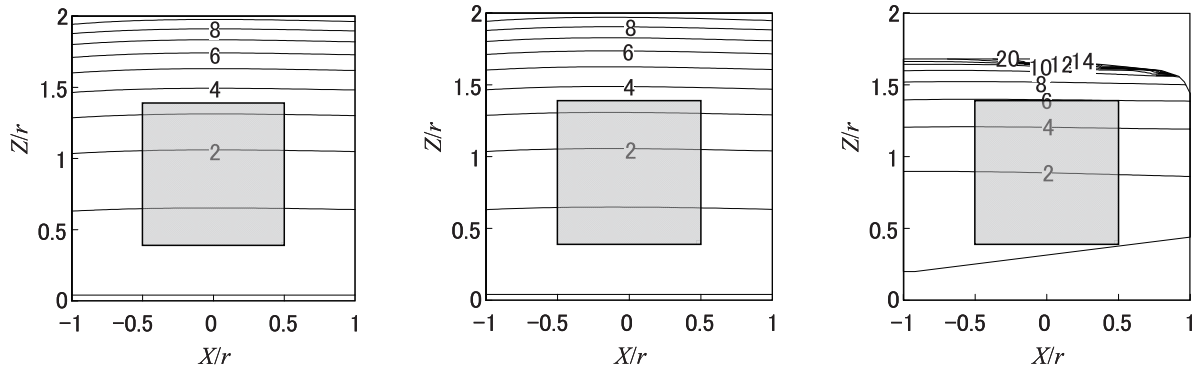

(a) $Y = 0$, $\theta_y = 0$, $\theta_z = 0$, $\psi = 0$ (b) $Y = -0.5r$, $\theta_y = 0$, $\theta_z = 0$, $\psi = 0$ (c) $Y = 0$, $\theta_y = -\pi/4$, $\theta_z = \pi/2$, $\psi = 0$

Fig. 10. Distribution of the determinant of the Jacobian matrix in the workspace of the mechanism designed.

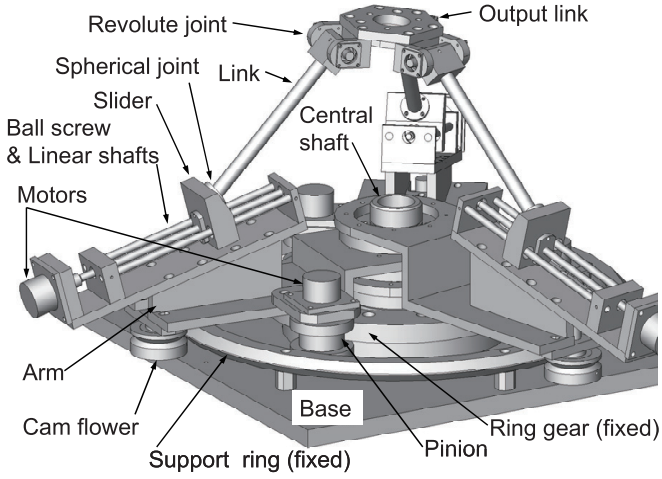

Fig. 11. 3D-drawing of the prototype 3-RPSR mechanism designed for a pipe bender.

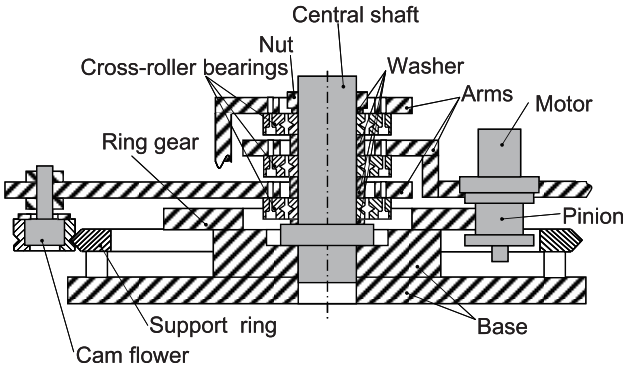

Fig. 12. Details of the triple revolute joints on the base and the supporting and driving parts of the arms.

5.2. Design Result

The design result is summarized in **Table 1**. Maps of the determinant of the Jacobian matrix in XZ cross sections are shown in **Fig. 10**. In these figures, the prescribed workspace is included in the square of side length r painted in grey. From these figures, it is evident that the kinematic characteristics of the mechanism designed do not change greatly, while the mechanism can achieve a large angle of orientation of the output link without reaching singularity (singularity: $\det J = 0$). Here, we evaluated the global stability of kinematic characteristics of the mechanism designed in the workspace using the determinant of the Jacobian matrix as an evaluation index, which is not homogeneous in terms of units. If the universal meaning of the value of the evaluation index is required, we should use a non-dimensional Jacobian matrix obtained by using a characteristic length [8].

5.3. Prototype Mechanism

Based on the results in 5.2, we designed the prototype mechanism. In the design, we evaluated, using the equations for static force analysis mentioned in section 4, force and moment at passive joints as well as driving force and torque at active joints for machining load exerted on the output link. A 3D-drawing of the prototype mechanism is shown in **Fig. 11**. Details of the triple revolute joints and the supporting and driving parts of the arms are shown by a cross-section view in **Fig. 12**. Photos of the prototype are shown in **Fig. 13**, where we can confirm that the prototype achieved a very large inclination angle of the output link ($\theta_y = 1.1$ rad). We observed that the prototype mechanism could rigidly keep its configuration against external load at highly inclined orientations, as shown in **Fig. 13 (b)**, as well as at the home pose, shown in **Fig. 13 (a)**.

6. Conclusions

In the present paper, we have proposed a new six-DOF parallel mechanism, a 3-RPSR mechanism with triple revolute joints on the base. Kinematic and static analyses were carried out, and a design example of this mechanism is shown. Our conclusions are summarized as follows.

(1) A new six-DOF parallel mechanism, 3-RPSR mechanism, composed of the base, output link, and three

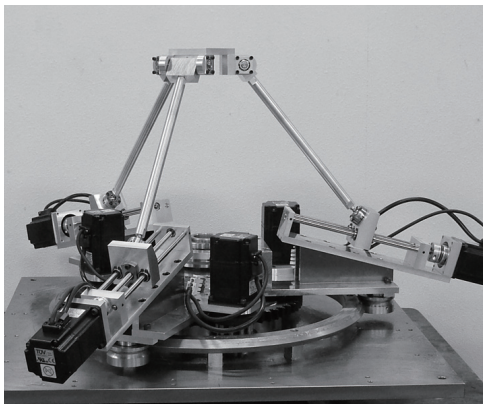

(a) Home pose

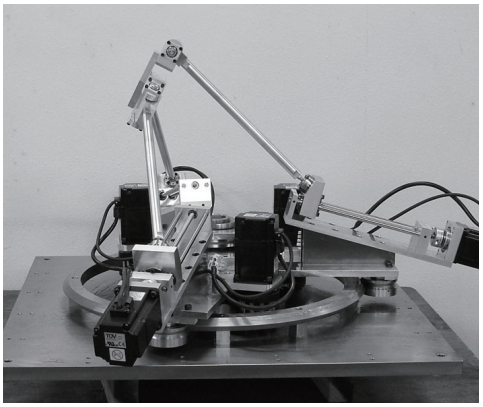

(b) Highly inclined orientation ($\theta_y = 1.1$ rad)

Fig. 13. Prototype 3-RPSR mechanism designed for a pipe bender.

RPSR chains with triple revolute joints on the base, is proposed. This mechanism can achieve a large angle of inclination and full rotation around the vertical axis of the output link.

(2) Equations for kinematic and static analyses of the 3-RPSR mechanism have been derived. The procedure to solve the inverse displacement analysis of this mechanism, including the discrimination of solutions, is clearly presented.

(3) Through the design and prototyping of a 3-RPSR mechanism with application to a pipe bender, we showed that the proposed mechanism can achieve a high orientation capability of the output link due to its structural feature and appropriate design.

References:

[1] Y. L. Chi, "Systems and methods employing a rotary track for machining and manufacturing," WIPO patent, No. WO 99/38646, 1999.

[2] http://mikrolar.com/rotopod.html

[3] Y. Takeda, K. Kamiyama, Y. Maki, M. Higuchi, and K. Sugimoto, "Development of position-orientation decoupled spatial in-parallel actuated mechanisms with six degrees of freedom," J. of Robotics and Mechatronics, Vol.17, No.1, pp. 59-68, 2005.

[4] M. Tanabe, Y. Takeda, and S. Huda, "Utility workspace of 3-5R translational parallel mechanism," J. of Advanced Mechanical Design, Systems, and Manufacturing, Vol.2, No.6, pp. 998-1010, 2008.

[5] S. Huda and Y. Takeda, "Kinematic analysis and synthesis of a 3-URU pure rotational parallel mechanism with respect to singularity and workspace," J. of Advanced Mechanical Design, Systems, and Manufacturing, Vol.1, No.1, pp. 81-92, 2007.

[6] M. Higuchi, R. Ishii, and Y. Takeda, "Development of gripping mechanism with large gripping force for a draw pipe bender which fabricates complex 3-dimensional shape pipes," Proc. of the 2009 JSME Conf. on Robotics and Mechatronics, 2A2-A17, 2009.

[7] J. Imoto, Y. Takeda, H. Saito, and K. Ichiryu, "Optimal kinematic calibration of robots based on maximum positioning-error estimation (Theory and application to a parallel-mechanism pipe bender)," Proc. of the 5th Int. Workshop on Computational Kinematics, pp. 133-140, 2009.

[8] M. Tandirci, J. Angeles, and F. Ranjbaran, "Characteristic point and the characteristic length of robotic manipulators," Proc. ASME DETC1992, DE, Vol.45, Robotics, Spatial Mechanisms, and Mechanical Systems, pp. 203-208, 1992.

Name:
Yukio Takeda

Affiliation:
Associate Professor of Mechanical Sciences and Engineering Department, Tokyo Institute of Technology

Address:
2-12-1 O-okayama, Meguro-ku, Tokyo 152-8552, Japan

Brief Biographical History:
1987 Graduated from Tokyo Institute of Technology
1989- Research Associate, Tokyo Institute of Technology
1996- Associate Professor, Tokyo Institute of Technology

Main Works:
• "A Spatial Six-Dof Parallel Manipulator with Redundant Actuators for Gross and Fine Motions," J. of Advanced Mechanical Design, Systems, and Manufacturing, Vol.4, No.2, pp. 444-456.

Membership in Academic Societies:
• The Japan Society of Mechanical Engineers (JSME)
• The Robotics Society of Japan (RSJ)
• The Japan Society for Precision Engineering (JSPE)

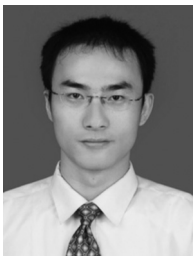

Name:
Xiao Xiao

Affiliation:
Sugimoto & Takeda Lab, Department of Mechanical Sciences and Engineering, Tokyo Institute of Technology

Address:
1-8-7 Kitamagome, Otaku, Tokyo, Japan

Brief Biographical History:
2007- Graduated from Dalian University of Technology
2007- Reserch student, Tokyo Institute of Technology
2008- Graduate student, Tokyo Institute of Technology

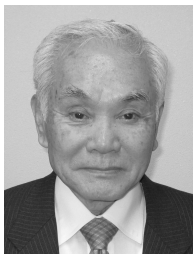

Name:
Kazuya Hirose

Affiliation:
Kikuchi Seisakusho, Co., Ltd.

Address:
2161-12 Miyama-cho, Hachioji-shi, Tokyo 192-0152, Japan

Brief Biographical History:
1967 Graduated from Yamagata University
1968-1982 Engineer, Union Carbide Corp. SEL
1982-2002 Engineer, Hephaist Seiko Co., Ltd.

Membership in Academic Societies:
- The Japan Society of Mechanical Engineers (JSME)
- The Japan Society for Precision Engineering (JSPE)

Name:
Yoshiki Yoshida

Affiliation:
Research Engineer, Kikuchi Seisakusho, Co., Ltd.

Address:
2161-12 Miyama-cho, Hachioji-shi, Tokyo 192-0152, Japan

Brief Biographical History:
2006- Kikuchi Seisakusho Co., Ltd.

Main Works:
- Development parallel Mechanism for precision stage, servo press, and motion bass.

Membership in Academic Societies:
- The Japan Society of Mechanical Engineers (JSME)
- The Japan Society for Precision Engineering (JSPE)

Name:
Ken Ichiryu

Affiliation:
Kikuchi Seisakusho, Co., Ltd.

Address:
2161-12 Miyama-cho, Hachioji-shi, Tokyo 192-0152, Japan

Brief Biographical History:
1959 Hitachi Research Lab., Hitachi Co., Ltd.
1981 Mechanical Engineering Lab., Hitachi Co., Ltd.
1986 Technical Research Center, Hitachi Construction Machinery, Co., Ltd.
1996 Professor, Tokyo University of Technology
2006 Manager, Research Lab., Kikuchi Seisakusho, Co., Ltd.

Main Works:
- Electro- Hydraulic Control, Nikkan Kogyo Shinbun, 1993, Ltd.

Membership in Academic Societies:
- Japan Society of Mechanical Engineers (JSME)
- Japan Society for Technology of Plasticity (JSTP)
- Japan Society for Precision Engineering (JSPE)
- Society of Automotive Engineers of Japan (JSAE)
- Robotic Society of Japan (RSJ)
- Water Jet Technology Society of Japan (WJTSJ)